Effect of machining processes on the residual stress distribution heterogeneities and their consequences on the stress corrosion cracking resistance of AISI 316L SS in chloride medium

Amir Ben Rhouma[1] · N. Sidhom[1] · K. Makhlouf[2] · H. Sidhom[1] · C. Braham[3] · G. Gonzalez[4]

Abstract
The effects of machining such as grinding and turning on the microstructural and mechanical changes of the machined surfaces of AISI 316L stainless steel (SS) have been studied. Surface aspects and surface defects have been examined by scanning electron microscopy (SEM). Machining-induced nanocrystallization has been investigated by transmission electron microscopy (TEM). Surface and subsurface residual stress distribution and plastic deformation induced by the machining processes have been assessed by X-ray diffraction (XRD) and micro-hardness measurements, respectively. The susceptibility to stress corrosion cracking (SCC) has been assessed by SEM examination of micro-crack networks which are characteristics of a machined surface immersed in boiling (140 ± 2 °C) solution of $MgCl_2$ (40%) during a 48 h-period. The machined surface properties have been correlated to severe plastic deformation (SPD) resulting from specific cutting state of each process. High cutting temperature and plastic rate are considered to be at the origin of near-surface austenitic grain refinement that leads to equiaxed nanograins with a size ranging from 50 to 200 nm. Ground surface residual stress distribution heterogeneities at the micrometric scale are attributed to the random distribution of the density and the geometry of abrasive grains that represent micro-cutting tools in the grinding process. The relationship between residual stress distribution and susceptibility of the AISI 316L SS to SCC has been demonstrated, and an experimental criterion for crack initiation has been established.

Keywords Stainless steel · Machining · Residual stress · Nanostructure · Chloride medium · Crack network · Stress corrosion cracking threshold

1 Introduction

It is well established that machining processes induce surface modifications of the upper layers of the surface as a result of the tool–material interactions. The integrity of the generated surface could be affected through roughness, hardness, nanostructure, machining defect changes, and residual stress distribution. These factors, depending on the material behavior under severe plastic deformation imposed by the cutting conditions, control the mechanical performance of the

✉ Amir Ben Rhouma
Amir.benrhouma@ensit.rnu.tn

N. Sidhom
naziha.sidhom@gmail.com

K. Makhlouf
kamel.makhlouf@issatso.rnu.tn

H. Sidhom
habib.sidhom@gmail.com

C. Braham
Chedly.BRAHAM@ensam.eu

G. Gonzalez
joseggr@unam.mx

[1] Laboratoire de Mécanique, Matériaux et Procédés (LR99ES05), ENSIT, Université de Tunis, 5 AV Taha Hussein Montfleury, 1008 Tunis, Tunisia

[2] Preparatory Insitute for Engineering Studies of Nabeul, LR18ES45, University of Carthage, 8000 Nabeul, Tunisia

[3] Laboratoire Procédés et Ingénierie en Mécanique et Matériaux (PIMM, CNRS UMR 8006), ENSAM, 151 Bd de l'Hôpital, 75013 Paris, France

[4] Instituto de Investigaciones en Materiales, UNAM, Apdo Postal 70-360, 04510 Mexico, D.F., Mexico

manufactured parts [1–4]. In fact, it has been shown that the greater the surface roughness, the lower the fatigue and the stress corrosion cracking (SCC) resistance of the manufactured part [5–9]. Crack growth rates have been reported to increase significantly when the surface hardness in cyclic loading conditions and in corrosive environment (e.g., that of the primary water conditions of pressurized water reactors) increases [10, 11]. Residual stress has been considered the most influential factor in fatigue and SCC resistance [1, 2, 5–9, 12]. It has been demonstrated that the fatigue life of austenitic stainless steel is lowered by a tensile residual stress distribution [7]. Moreover, their susceptibility to SCC increases significantly by the synergetic effect of machining tensile residual stresses and chloride ions [5, 6]. However, the compressive residual stress improves the fatigue life [7] as well as the SCC resistance of austenitic stainless steels [5, 6]. Thus, residual stress has been recognized to play a major role in the nucleation and growth of fatigue and stress corrosion cracks. Indeed, a threshold value of the applied stress required to initiate SCC established by static tensile tests in corrosive media has been controversial due to some discrepancies related to the residual stress levels resulting from the sample preparation modes [13, 14]. Beavers et al. [15] presented an empirical correlation between residual stress level and stress corrosion cracking colonies in pipeline steel. However, this correlation does not seem to be obvious for the stress corrosion micro-crack distribution and density in austenitic stainless steel which results from machining-induced surface residual stress. This suggests the possible correlation of the scale of the stress corrosion cracking colonies with that of the machining-induced tensile residual stress level. Nevertheless, some controversial results related to the effect of the scale and the gradient of machining-induced residual stress on the fatigue and the stress corrosion crack nucleation at the surface of manufactured parts have not still been resolved in the published literature. Residual stress gradient and the scale of plastic deformation heterogeneities induced by machining processes could be at the origin of the misinterpretation of the stress corrosion crack network characteristics.

The aim of this study is to explore the correlation between machining processes and surface residual stress heterogeneity scale and their consequences on the stress corrosion micro-crack distribution in the near machined surface of the AISI 316L austenitic stainless steel in chloride medium. The turned and ground surfaces before and after SCC tests in boiling $MgCl_2$ solution were subjected to scanning electron microscopy (SEM) examination in order to establish the correlation between the scale of the machining-induced residual stress level and the stress corrosion micro-crack distributions. Machining-induced residual stress and their relaxation by stress corrosion crack initiation and growth were assessed by X-ray diffraction (XRD) measurements. The correlation with crack network leads to the determination of a threshold residual stress corrosion cracking (RSCC) value for AISI 316L stainless steel (SS) in boiling chloride medium $MgCl_2$ (40%) at 140 °C. This critical value of residual stress evaluates the susceptibility of the machined surface to stress corrosion (SC) micro-crack initiation regardless the material scale.

2 Material and experimental methods

The most used material for manufacturing nuclear power plants components is the austenitic stainless steel AISI 316L, which is used in this study. The chemical composition and the mechanical properties of this material are reported in Tables 1 and 2, respectively. The microstructure of the steel is fully austenitic with an average grain size of 60 μm resulting from a solution annealing at 1050 °C for 2 h followed by air cooling. Two machining processes such as grinding and turning are applied as surface preparation modes for the AISI 316L SS.

Samples used in this study are 20 × 20 × 5 mm plates for the grinding process and 50-mm diameter and 20-mm-long rings for the turning process. The applied cutting conditions and the used tool characteristics are reported in Table 3. The studied zones have been randomly selected and numbered on the machined surface in order to investigate the heterogeneity scale of the surface integrity characteristics before and after the SCC tests (Fig. 1a, b). The surface aspects of each zone are identified by SEM examinations and correlated with the specific tool–material interactions under different machining conditions (Table 3). The machining-induced surface residual stress for each investigated zone was measured by using XRD method with the selected experimental conditions as reported in Table 4. The electropolishing method is used to investigate the in-depth residual stress distribution. The directionality and the gradient of machining-induced residual stresses are determined by using profiles obtained by measurements in both the cutting and the perpendicular directions. By combining the KαMn and the KαCu radiations, the gradient of residual stresses, including 2-μm-deep values, was also obtained by XRD method. Measurements are carried out before and after SCC tests in order to evaluate the stress relaxation related to crack network characteristics. The machining-induced microstructure changes were investigated using TEM type JEOL 120EX. Thin foils are taken from a plane perpendicular to the

Table 1 Chemical composition of AISI 316L SS (wt%)

C	Si	Mn	P	S	Cr	Ni	Mo	N	Cu	V	Fe
0.02	0.56	1.67	0.041	0.041	17.24	11.14	1.96	0.066	0.35	0.055	Balance

Table 2 Mechanical characteristics of AISI 316L SS in annealing state

Yield stress (MPa)	Ultimate tensile stress (MPa)	A (%)	Micro-hardness ($HV_{0.05}$)
200	535	70	190

turned surface using the focused ion beam equipment (model FIB JEOL JEM-9320). The plastic deformation resulting from cutting processes is quantified using micro-hardness measurements conducted on the machined surface cross-section.

The stress corrosion cracking tests are carried out by an accelerated immersion of machined samples in boiling (140 ± 2 °C) solution of $MgCl_2$ (40%) for a period of 48 h. The residual stress–induced crack network related to the different numbered zones was identified by optical and SEM examinations of SCC-tested surfaces. The effect of the temperature and the medium on the relaxation of the machining-induced residual stress has been assessed by XRD measurements conducted on the ground surface before and after holding the sample for 48 h at a temperature of 140 °C in air medium.

3 Results

3.1 Machined surface properties

3.1.1 Machining-induced plastic deformation

SEM examination of machined surfaces reveals a specific texture corresponding to the tool–material interaction mode, depending on the process type and the local geometry of the tool as shown in Fig. 2a, b for ground and turned surfaces, respectively. The machined surface texture recounts the markings of the tool penetration under the engaged cutting force as a result of the sample material plastic flow. Therefore, the extent of plastically deformed zone is compared with the tool–material contact area that depends on the tool geometry, specifically on the nose radius and the cutting edge angles and on the engaged cutting force. Indeed, the scale of the deformed zone by the grinding process is around 200 μm corresponding to the dimension of the penetration depth of the abrasive grain size. The adjacent abrasive grain with different cutting edges could induce a deformed zone with higher or lower plastic deformation level and consequently different penetration depth as shown in SEM micrographs (zones 1 and 2 in Fig. 2a). However, the plastically deformed zone induced by turning is lower than 0.5 mm and corresponds to the cutting tool–sample material contact area (Fig. 2b). Therefore, the scale of plastic deformation heterogeneity on the machined surface is in the same order of magnitude as the area corresponding to the contact tool–sample material under the engaged cutting force. This force depends on the cutting conditions and could affect the machined surface residual stress distribution. Finally, based on the machined surface aspect, it can be expected that the scale of the grinding-induced plastic deformation is some orders of magnitude lower than that of the turning one.

Furthermore, the work hardening induced by machining processes is assessed experimentally by cross-section micro-hardness measurements, showing increased values up to 480 $HV_{0.05}$ for the turned surface and to 280 $HV_{0.05}$ for the ground surface compared with 180 $HV_{0.05}$ for the bulk material. The high level of the micro-hardness is associated with plastic deformation revealed by optical microscope examination of the cross-section showing slip bands near the machined surface (Fig. 3). Moreover, the micro-hardness profiles show larger plastically deformed layers by the turning process (0.5 mm) compared with the grinding process (0.2 mm).

3.1.2 Machining-induced nanostructure

Transmission electron microscopy (TEM) micrographs show that machining operation induced a severe plastic deformation (SPD) generating a progressive refinement of the grains over a region of few microns below the surface (Fig. 4). The nanometric grained structure is observed within the near-surface layer of 1 to 3 μm in thickness. This nanostructure, composed of randomly distributed equiaxed grains with sizes varying from 50 to 200 nm, is encountered by deformed grains characterized by high dislocation densities (Fig. 4a). The electron diffraction patterns show almost continuous diffraction rings coming from the nanostructured layer formed by randomly oriented grains (Fig. 4b). The characteristics of the nanostructure, such as the size of the nanograins and the extent of the nanostructured layer, depend on the cutting conditions

Table 3 Cutting conditions

Grinding			Turning			
Grinding wheel	Feed rate V_w (m/min)	Grinding depth a (μm)	Radius of the tool nose $R\varepsilon$ (mm)	Feed rate f_n (mm/rev)	Cutting speed V_c (m/min)	Depth of cut a_p (mm)
99A46H7VNE	4	10	0.8	0.4	150	2

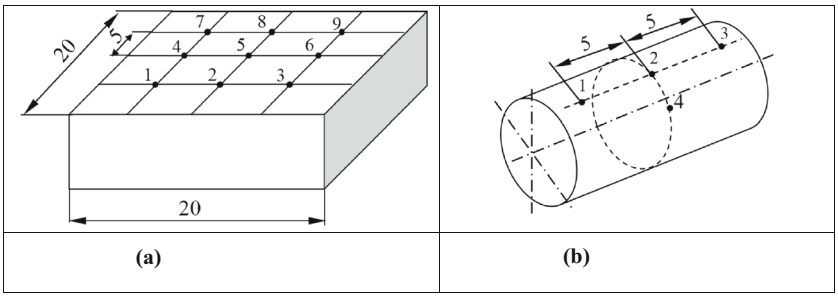

Fig. 1 Investigated zones of the machined surface: **(a)** ground surface; **(b)** turned surface

controlling the temperature, the plastic strain rate, and the plastic velocity.

3.1.3 Machining-induced residual stress

The near-surface distribution of the machining-induced residual stress is evaluated by XRD method. The measurements assess the arithmetic average stress in the volume of irradiated zone defined by the X-ray beam diameter which is set at 2 mm and a penetration depth into austenitic stainless steel ranging from 5 to 10 μm. Surface residual stress values corresponding to measurements in parallel and perpendicular directions to machining striations for various marked areas (shown in Fig. 1a, b) are reported in Table 5 where errors in measurements are also listed. Results show an important heterogeneity of residual stress distribution on the ground surface which exceeds experimental measurement scattering that could be related to plastic deformation heterogeneity. The measured stress varies from + 141 to + 473 MPa in the grinding direction and from − 157 to + 254 MPa in the transverse direction depending on the marked zone as shown in Fig. 1a. However, turning-induced residual stress appears to be similar for the four different marked zones (Fig. 1b). This indicates a homogeneous distribution for this process, as expected from the scale of plastic deformation homogeneity. It is important to notice that residual stresses in the machining direction (parallel to machining striations) are all tensile (positive values) and vary from + 797 to + 892 MPa whereas in the perpendicular direction, stresses are at lower values varying from + 205 to + 337 MPa. The in-depth measurements of residual stress, using the KαMn radiation, reveal a gradient of tensile stress from 670 MPa near the surface to 250 MPa at a depth of 200 μm as highlighted by the profile reported in Fig. 5a. Moreover, the measurements using the KαCu radiation reveal an important gradient of residual stress in the extent of the first 2 μm from the surface where a value of stress in the grinding direction of 1206 ± 80 MPa at 1.5 μm from the surface is measured (Fig. 5b).

Table 4 Experimental conditions of X-ray diffraction (XRD)

Parameter	Set parameter				
Radiation	λMnK$\alpha \times \lambda = 0.2102$ mm				
Voltage	20 KV				
Current	5 mA				
XRD planes	(3 1 1) $2\theta \approx 152°$				
Beam diameter	2 mm				
Φ angles (°)	0 and 90				
ψ oscillation	± 3°				
ψ angles (°)	− 42.95	− 38.81	− 34.54	− 30.00	− 25.00
	− 19.11	− 10.89	0.00	15.50	22.21
	27.58	32.31	36.70	40.89	45.00

3.2 Susceptibility to stress corrosion cracking

3.2.1 Morphology of micro-crack network

The SEM examinations of machined sample surfaces after immersion in boiling (140 ± 2 °C) $MgCl_2$ (40%) solution for 48 h reveal a stress corrosion micro-crack network indicating a susceptibility to SCC of AISI 316L SS. The distribution and morphologies of micro-cracks could be correlated to the machining-induced residual stress distribution as indicated by SEM observation results summarized in Table 5 and corresponding to different market zones after SCC tests. It has been established that stress corrosion crack networks characterized by short and long micro-cracks in the uniaxial and biaxial configurations depend on the surface distribution of the machining-induced residual stresses. Indeed, it has been clearly shown that the micro-crack density increases significantly with increasing the tensile level of the residual stress for both ground and turned surfaces (Fig. 6). Moreover, the long cracks are usually oriented perpendicular to the high value of tensile residual stress while the shorter ones, where they exist, are perpendicular to the low tensile residual stress, thus ensuring a continuous biaxial crack network (Fig. 6a, b). The unidirectional micro-crack distribution is observed when one component of the residual stress field is compressive or has a low tensile value (Fig. 6c, d). However, the marked zones on the turned surface reveal a continuous biaxial micro-crack network related to the high level of surface tensile stresses. Indeed, nucleation and growth of micro-cracks are observed in both directions corresponding to stress levels higher than

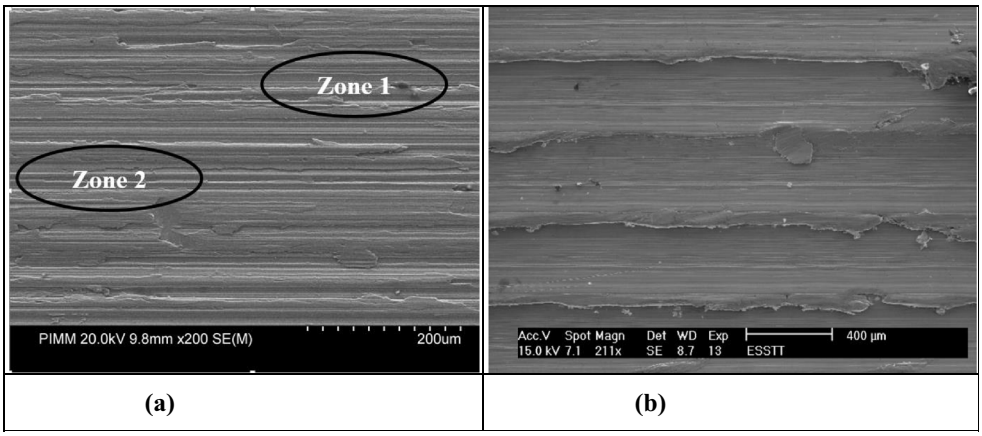

Fig. 2 Aspect of machined surface resulting from tool–material interactions under different cutting processes: **(a)** ground surface; **(b)** turned surface

800 MPa in the circumferential direction and higher than 300 MPa in the longitudinal one (Fig. 6e, f). In addition, the depth of stress corrosion micro-cracks varies from 0.4 to 1.5 mm (Fig. 7) which is considered to be higher than the width of the tensile residual stress profile which varies from 0.2 to 0.4 mm.

3.2.2 Residual stress corrosion cracking threshold

The analysis of XRD measurements and SEM examination results, as reported in Table 5, reveals a relationship between residual stress distribution and susceptibility to SCC. Indeed, the marked zones G17, G18, and G19 of ground surfaces are free from cracks, which coincides with relatively low values of tensile residual stresses (($\sigma_{11} = 188$ MPa; $\sigma_{22} = -105$ MPa), ($\sigma_{11} = 316$ MPa; $\sigma_{22} = -55$ MPa), ($\sigma_{11} = 141$ MPa; $\sigma_{22} = -157$ MPa)). However, the remaining zones seem to be sensitized to SCC. This suggests that a threshold stress corrosion cracking value that takes into account the level and the directionality of machining-induced residual stress should be considered. The SEM observations (cracking/no cracking) of tested SCC samples in the biaxial residual stress diagram σ_{11}-σ_{22} prove the existence of two domains with a straight line separating micro-crack existing zone and crack-free zone (Fig. 8). This diagram correlates the residual stress distribution with the susceptibility to SCC for the AISI 316L SS in chloride medium at 140 °C. Therefore, an experimental criterion to SCC susceptibility taking into account the level and the directionality of residual stresses can be expressed as follows:

$\sigma_{11}^{R} + \sigma_{22}^{R} < \left(\sigma_{\text{threshold}}^{\text{RSCC}}\right)_{MgCl_2;40\%;140°C}$ with a threshold value of residual stress $\left(\sigma_{\text{threshold}}^{\text{RSCC}}\right)_{\text{MgCl}_2;40\%;140°C} = 270$ MPa

3.2.3 Residual stress relaxation

To evaluate the effects of SCC test temperature (140 °C) and medium on the relaxation of machining-induced residual stresses, measurements are carried out on the ground surface samples which are tested with and without corrosive medium and compared with the previous tests. Results reported in Table 6 show that the temperature of the medium (140 °C) could provoke a slight relaxation of residual stresses evaluated at 20 to 50 MPa which are insignificant taking into account measurement uncertainty as shown in column 5 of Table 6. However, nucleation and growth of micro-cracks result in an important decrease of residual stress with a rate reaching 80% in the cutting direction and 270% in the perpendicular direction, as indicated in column 3 of Table 6. This relaxation can influence the in-depth propagation of stress corrosion micro-cracks.

4 Discussion

4.1 Correlation between machining processes and properties of affected layers

The analyses of AISI 316L SS machined surface results from microstructural and mechanical investigations carried out on ground and turned samples demonstrate that the involved cutting force and the dissipated thermal energy induced by material sample and tool interactions lead to significant surface modifications. These modifications include roughness, nanostructure, plastic deformation, and residual stress distribution. It has also been established that surface changes take place in the near-surface layers reaching 200 µm for the ground surfaces and 400 µm for the turned surfaces depending on the cutting conditions. These results are in good agreement with those of previous research work conducted on the AISI 316L SS [5, 6].

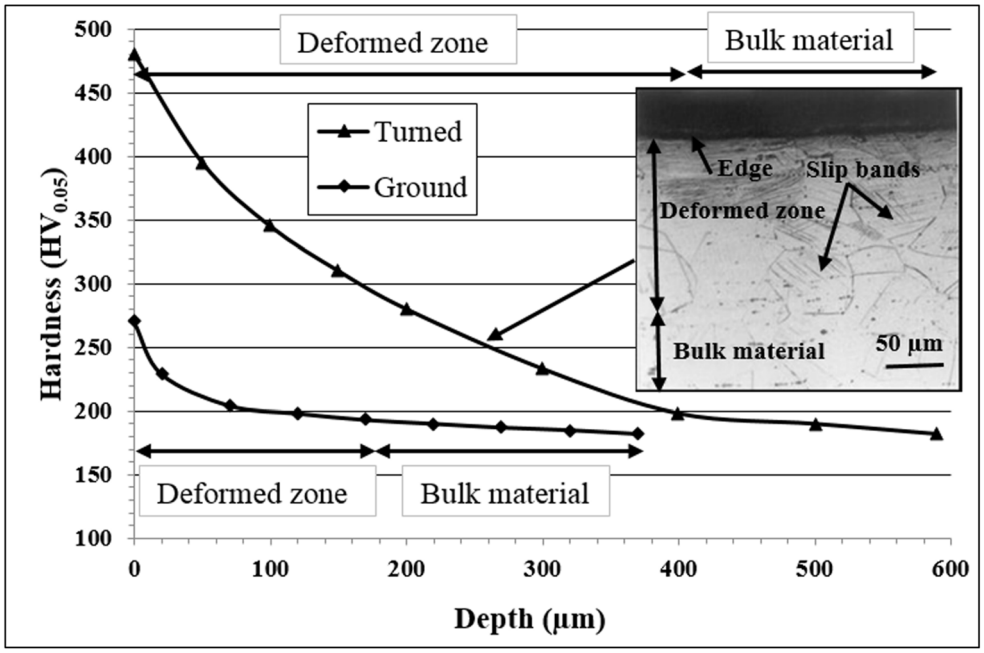

Fig. 3 Surface hardening resulting from machining-induced plastic deformation

The results of this study confirm the heterogeneities of the microstructure, the residual stress, and the plastic deformation of the surface and underneath the surface of the sample, as reported in experimental and numerical machined surface investigations found in the literature [16, 17].

4.1.1 In-depth heterogeneity

The experimental profiles of micro-hardness (Fig. 3) and residual stress (Fig. 5) established in this study indicate that a gradient of machining-affected layer properties could be correlated to the microstructure gradient that is revealed by micro-scale (Fig. 3) and nanoscale (Fig. 4) investigations. Indeed, the hardness gradient is due to surface nanostructured layers generated at the near surface (Fig. 4) and to the highly deformed under layers (Fig. 3). The shallow depth of nanocrystalline structure was considered to be the result of the severe near-surface plastic deformation (SPD) induced by machining processes [18, 19]. The in-depth slip bands and elongated grains are related to conventional plastically deformed material under machining conditions [1, 20]. The relationship between microstructure and hardness gradient resulting from machining has also been reported in other studies on austenitic stainless steels types 304 and 316, showing a decrease in micro-hardness with increasing the depth. These

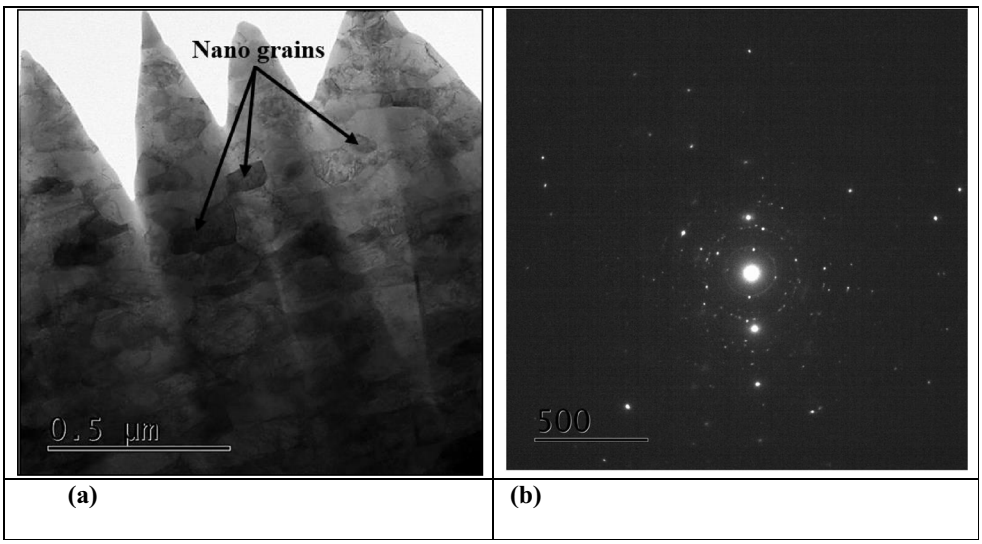

Fig. 4 Grain refinement resulting from severe plastic deformation (SPD) induced by the turning process: **(a)** nano-grains (50 nm to 200 nm); **(b)** diffraction patterns showing continuous rings related to nanostructure

Table 5 Correlation between induced-residual stress and susceptibility to SCC of AISI 316L SS in $MgCl_2$ (40% - 140 °C) medium

Sample condition	Investigated zone	Induced residual stresses		Susceptibility to SCC	Morphology of crack network
		σ_{11} (MPa)	σ_{22} (MPa)		
Surface ground	G.11	355 ± 17	110 ± 9	Cracks	Biaxial
	G.12	473 ± 11	156 ± 15	Cracks	Biaxial
	G.13	372 ± 15	85 ± 15	Cracks	Uniaxial
	G.14	395 ± 13	254 ± 9	Cracks	Biaxial
	G.15	394 ± 15	173 ± 12	Cracks	Biaxial
	G.16	252 ± 11	24 ± 9	Cracks	Uniaxial
	G.17	188 ± 25	− 105 ± 18	No cracks	–
	G.18	316 ± 29	− 55 ± 12	No cracks	–
	G.19	141 ± 14	− 157 ± 1	No cracks	–
Surface turned	T.1	832 ± 34	216 ± 35	Cracks	Biaxial
	T.2	882 ± 37	337 ± 29	Cracks	Biaxial
	T.3	892 ± 34	218 ± 33	Cracks	Biaxial
	T.4	797 ± 29	205 ± 35	Cracks	Biaxial

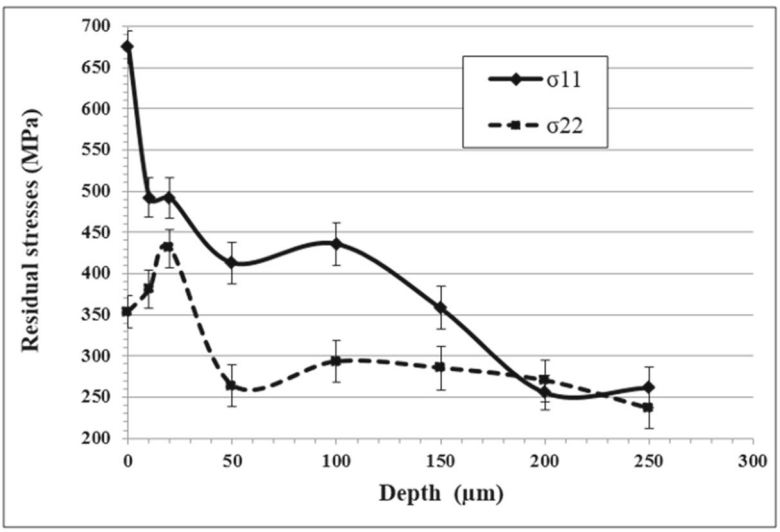

(a)

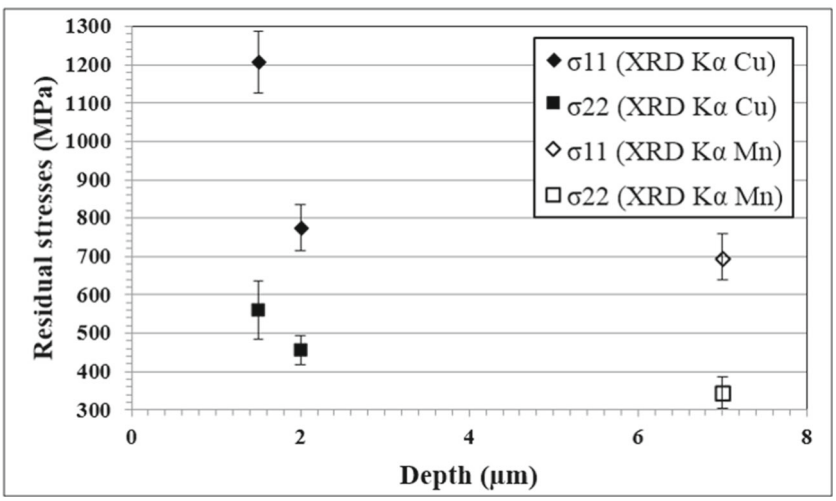

(b)

Fig. 5 Grinding-induced residual stress gradient: **(a)** XRD using KαMn radiation and electropolishing method; **(b)** XRD using KαMn radiation in near surface and KαCu radiation in depth

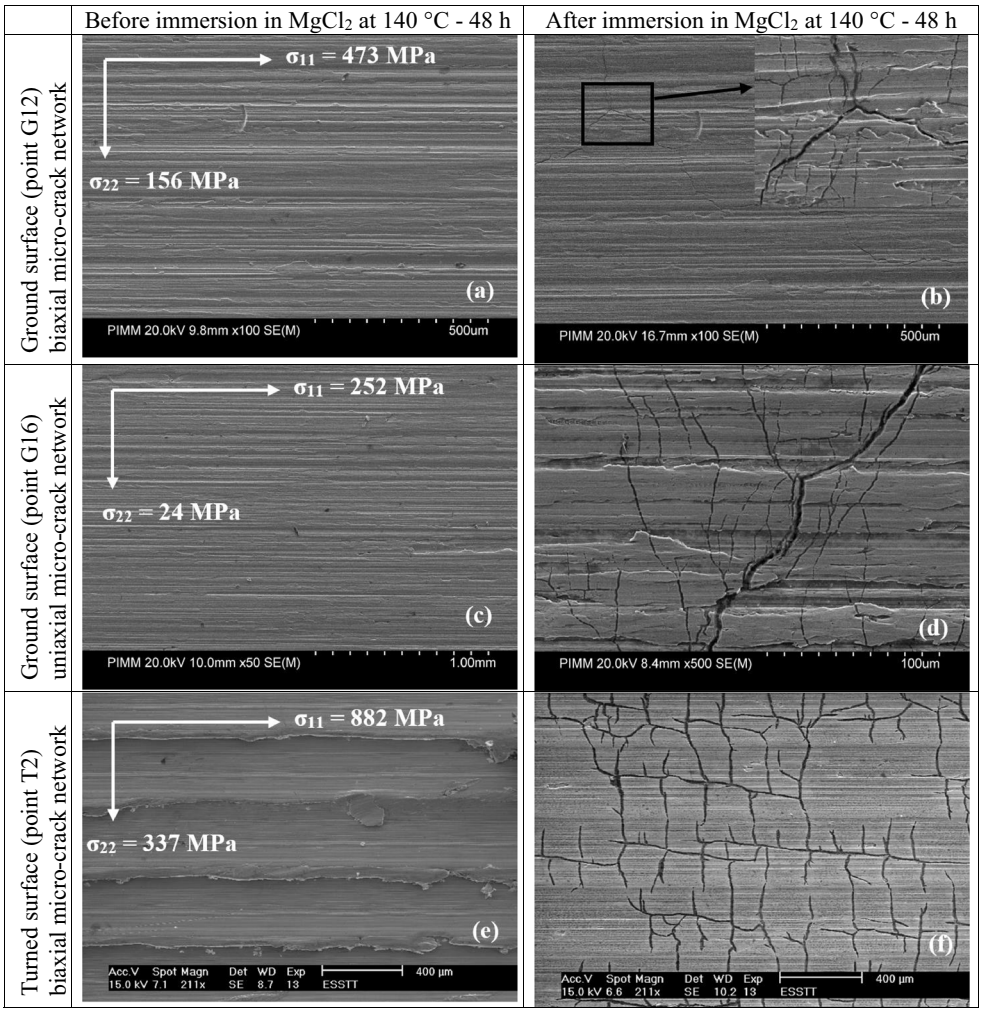

Fig. 6 Effect of tensile residual stress directionality on the morphology of stress corrosion micro-crack networks

hardness values vary from 350 $HV_{0.05}$ on the surface to 220 $HV_{0.05}$ in depth for the AISI 304 SS [7] and from 380 $HV_{0.05}$ to 180 $HV_{0.05}$ for the AISI 316L SS [6]. On the other hand, residual stress gradient generated by both grinding and turning processes is characterized by high levels of tensile residual stresses and plastic deformation

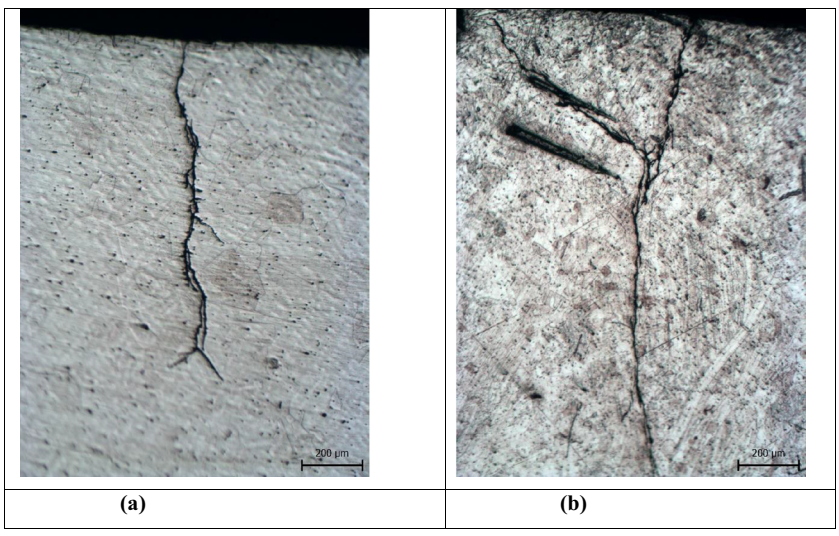

Fig. 7 In-depth propagation of stress corrosion micro-cracks: **(a)** ground surface; **(b)** turned surface

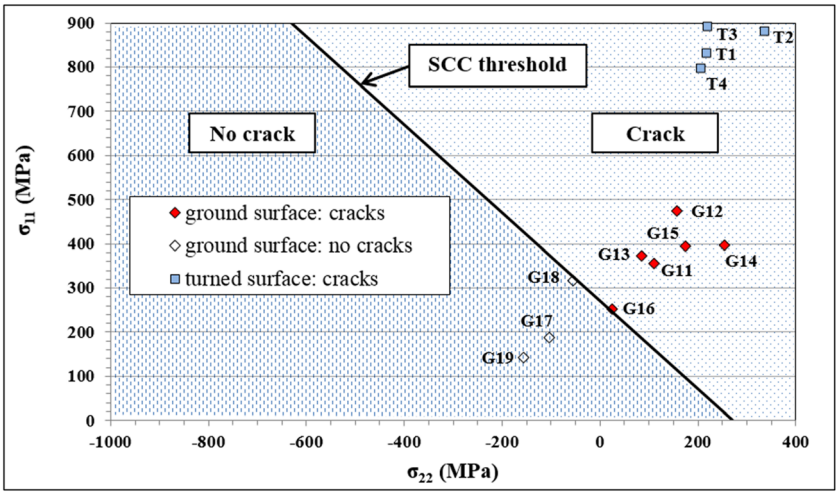

Fig. 8 Criterion to SCC susceptibility of AISI 316L SS in chloride medium ($MgCl_2$; 40%) at 140 °C

(Figs. 4 and 5) on the upper layers of the material. These values decrease at the under layers due to significant mechanical and thermal gradients resulting from the machining operations. Furthermore, in the turning process, the value of tensile residual stress has a higher value in the cutting direction than in the perpendicular one. However, in the grinding process, tensile residual stresses are usually observed parallel to the cutting direction. In perpendicular direction, these residual stresses become less tensile or even compressive. Moreover, it has been clearly established that the residual stress gradient is strongly pronounced at a depth less than 2 μm from the ground surface (Fig. 5b). For the turned surface, the same phenomenon is expected to exist in the near surface but it is difficult to investigate by using grazing incidence XRD method due to the high roughness of the surface compared with the ground one. The grain refinement and the high dislocation density identified by TEM examination (Fig. 4a) are considered to be responsible for the pronounced residual stress gradient in the near-surface zone [18, 19]. Similar results are reported by several researchers who attributed the profiles of machining-induced residual stresses to the effect of thermal and mechanical interactions between tool and sample material even if the relative significance varies from one process to another [12, 21–23]. In most types of machining, heat is generated on the surface of the sample and subsequent cooling produces contraction of the surface layers, which is

Table 6 Effects of SCC and test temperature (140 °C; 48 h) on the residual stress relaxation on the ground surface

Specimen immersed in an aggressive medium: $MgCl_2$							Specimen placed in a neutral medium: air						
	Column 1		Column 2		Column 3			Column 4		Column 5		Column 6	
Investigated zone	Induced residual stresses		Effect of SCC test		Relaxation rate		Investigated zone	Induced residual stresses		Effect of test temperature		Relaxation rate	
	σ_{11} (MPa)	σ_{22} (MPa)	σ_{11} (MPa)	σ_{22} (MPa)	σ_{11} (%)	σ_{22} (%)		σ_{11} (MPa)	σ_{22} (MPa)	σ_{11} (MPa)	σ_{22} (MPa)	σ_{11} (%)	σ_{22} (%)
G.11	355 ± 17	110 ± 9	267 ± 6	71 ± 12	25	35	G.21	220 ± 48	− 173 ± 42	186 ± 50	− 167 ± 38	15	3.5
G.12	473 ± 11	156 ± 15	101 ± 10	− 117 ± 12	78	175	G.22	691 ± 34	306 ± 24	668 ± 39	239 ± 40	3.5	22
G.13	372 ± 15	85 ± 15	93 ± 22	− 91 ± 17	75	207	G.23	112 ± 55	− 246 ± 36	95 ± 56	− 234 ± 35	15	5
G.14	395 ± 13	254 ± 9	346 ± 7	138 ± 39	12	45	G.24	717 ± 41	534 ± 35	675 ± 50	501 ± 34	6	6
G.15	394 ± 15	173 ± 12	211 ± 9	− 63 ± 9	46	136	G.25	675 ± 48	354 ± 41	645 ± 43	312 ± 39	4.5	12
G.16	252 ± 11	24 ± 9	167 ± 40	− 41 ± 33	34	270	G.26	489 ± 44	210 ± 28	475 ± 44	171 ± 33	3	19
G.17	188 ± 25	− 105 ± 18	169 ± 31	− 165 ± 25	10	57	G.27	851 ± 51	483 ± 44	815 ± 47	483 ± 34	4	0
G.18	316 ± 29	− 55 ± 12	298 ± 24	− 69 ± 18	37	25	G.28	294 ± 25	− 205 ± 35	234 ± 34	− 198 ± 48	20	3.5
G.19	141 ± 14	− 157 ± 1	106 ± 25	− 199 ± 9	25	21	G.29	339 ± 39	21 ± 35	325 ± 35	1 ± 34	4	5

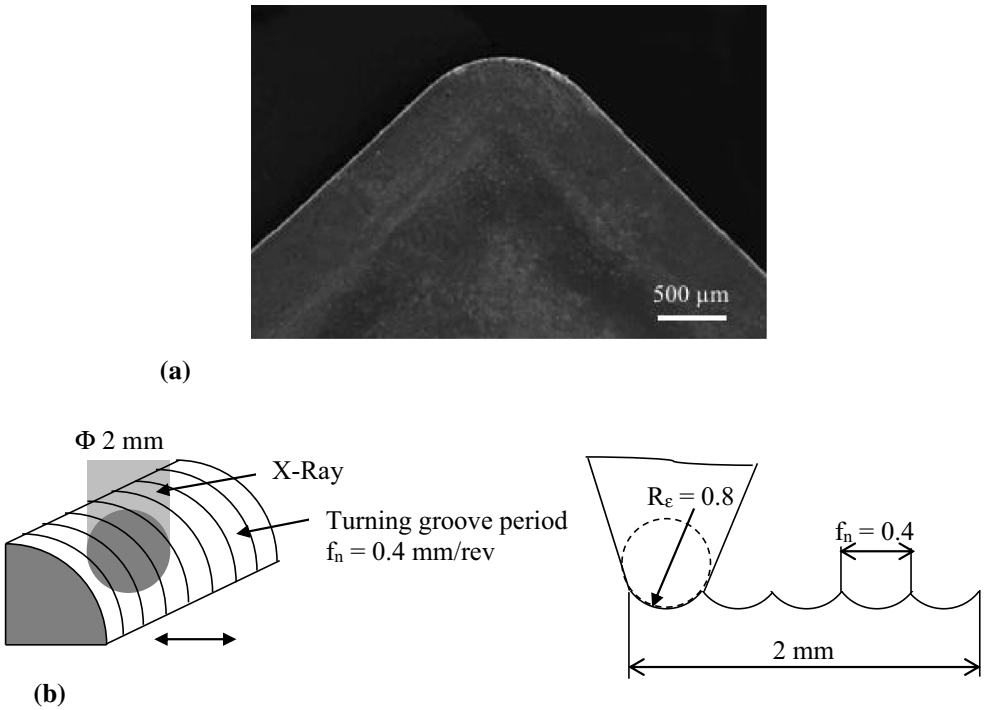

Fig. 9 Cutting edge image and turned area scheme covered by the X-ray irradiation during residual stress measuring: **(a)** cutting edge of the cutting tool used for turning experiment; **(b)** interaction tool–material zone in the turning process compared with X-ray irradiation zone corresponding to X-ray measurements of residual stress

hampered by the bulk material leading to a tensile residual stress at the surface balanced by a compressive residual stress in the subsurface. Therefore, the anisotropic surface and subsurface configurations of the residual stress distribution shown in this study can be attributed to the anisotropic plastic deformation of the machined surface layer. This indicates that residual stresses induced by mechanical effects dominate over isotropic thermal effects, as found in this study and in other studies for the case of AISI 304 SS ground surface [24, 25].

4.1.2 On the surface heterogeneity

Previous works related to machining-induced residual stress distribution in metallic alloys prove the significant effects of sample material behavior and interrelated process parameters such as cutting speed, feed rate, depth of cut, and tool type and geometry. Moreover, it has been established that all factors that control the cutting state at different scales of the machined surface could affect the residual stress distribution [6, 12, 26–29]. Indeed, the vibrations of the machine and the tool, which can provoke instantaneous modification of cutting depth and speed, influence the residual stress distribution [30]. The tool wear resulting in tool edge geometry changes also affects the residual stress distribution as a consequence of the related local modification of cutting forces, temperature, and applied stress [31–34]. Furthermore, the cooling mode, through its efficiency to dissipate the energy converted into heat on the machined surface, is considered by other authors [2, 28, 35] as a main factor controlling the residual stress distribution.

The measured residual stresses on the turned and ground surfaces of AISI 316L SS confirm the established literature results relating all factors controlling the machining-induced residual stress. However, the heterogeneity of measured values of residual stress on the ground surface, exceeding the usual discrepancy phenomenon as shown in Section 3.1.3, suggests an effect of the heterogeneity of local cutting state at the scale of the tool–material interaction area which is different for grinding and for turning. Indeed, the resulting tool–material contact area in the turning process, with 0.8-mm radius of the cutting tool (Fig. 9a), generates relatively homogeneous mechanical and thermal interactions covering a large fraction of the X-ray irradiated area of 2 mm in diameter Fig. 9b. This explains the more regular and constant measured residual stresses through the machined surface as illustrated in Table 5. On the other hand, in the grinding process, the heterogeneity of the abrasive grain density, which depends on the wheel type, on the grain size that varies from 290 to 550 µm, and on their respective cutting edge and radius (Fig. 10), generates a heterogeneous cutting state at the micrometric scale. This results in the revealed heterogeneity of residual stress on the ground surface as illustrated in Table 5. Therefore, for the ground surface, the cutting force and the friction of the micro-tool flank at the abrasive grain

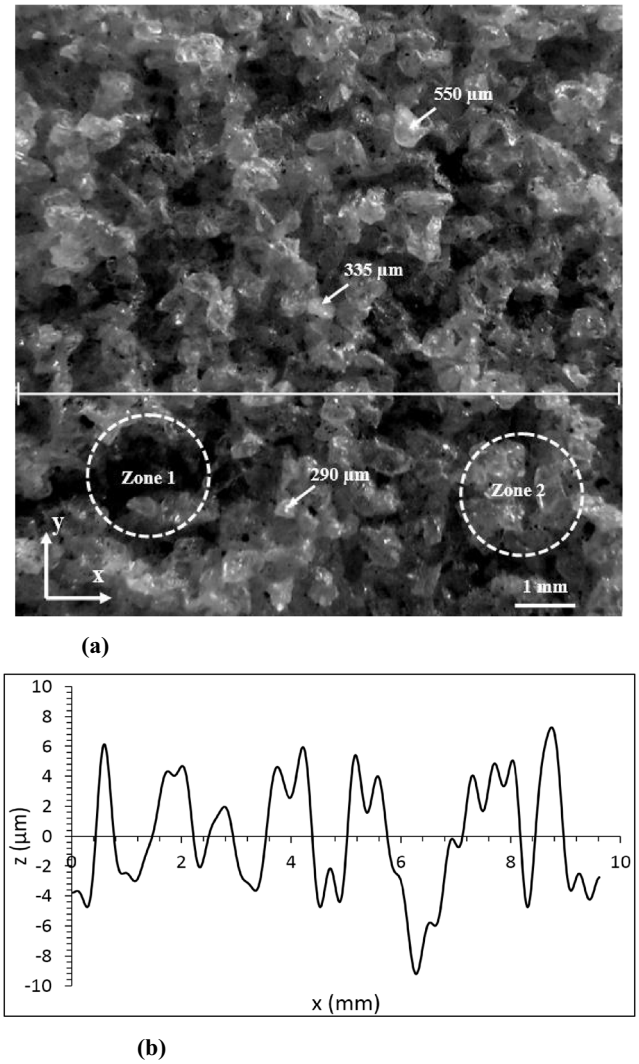

Fig. 10 Heterogeneities of abrasive grain density and geometry on the grinding wheel working surface: (**a**) image of the grinding wheel working surface; (**b**) grinding wheel roughness profile

scale added to the distribution of abrasive grain density of the grinding wheel could modify the induced plastic strain and the generated heat. This results in the heterogeneous distribution of residual stress, as expected by comparing zones 1 and 2 which correspond to the grinding wheel (Fig. 10a) and consequently to the ground surface (Fig. 10b).

4.2 Correlation between machined surface properties and stress corrosion micro-crack network

The performed RSCC tests reveal the susceptibility of the AISI 316L SS to stress corrosion micro-cracking in the chloride medium $MgCl_2$ (40%) at 140 ± 2 °C (Fig. 6). The initiation and growth of micro-cracks depend on the tensile residual stress level and distribution, which in turn depend on the surface preparation mode and conditions, as shown in this study by comparing the corrosion crack networks of turned and ground surfaces. However, for both machining processes, it has been established that a biaxial distribution of corrosion micro-cracks is systematically related to a biaxial field of surface residual stress. The relationship between the directionality of the tensile residual stress and the micro-cracks has been qualitatively demonstrated by Zhou et al. [25] in the case of AISI 304L SS in boiling $MgCl_2$. However, the result of this study establishes a quantitative criterion for the susceptibility of AISI 316L SS to SCC, taking into account the level and the directionality of the residual stress distribution. The criterion expressed as the trace of the residual stress tensor, which is less than a threshold value of 270 MPa, is required to prevent the micro-crack initiation in the chloride medium ($MgCl_2$; 40%) at 140 °C. These experimental results are confirmed after adding experimental data from previous studies found in the literature [6], as shown in Fig. 11. It is also consistent with literature results reporting a threshold value of 190 MPa for AISI 304 SS in the chloride medium ($MgCl_2$; 40%) at 155 °C [12]. Moreover, using this criterion, the distribution of sensitized areas of the AISI 316L SS ground surface could be explained, and thus, the different configurations of micro-crack networks will be easily commented. Indeed, the free crack area is systematically related to the trace of the residual stress tensor which is lower than the threshold value. The uniaxial corrosion micro-crack network was explained by a residual stress level in the cutting direction higher than the threshold crack initiation value (Fig. 6d). This directionality of the micro-cracks initiating on the machined surface as a result of high tensile residual stresses in the machining direction was observed earlier by several investigators [5, 6, 12]. Therefore, the heterogeneity, at the micrometric scale, of residual stress distribution on the ground surface is at the origin of the distribution of the corrosion micro-crack network morphology [1, 5, 6, 12, 25]. These results corroborate the commonly accepted role of the tensile residual stress distribution acting as the main driving force for micro-crack initiation on the surface layers. The well-accepted mechanism of crack initiation is a combination of tensile stress concentration and a more aggressive environment in surface defects such as machining groves. At the microscopic scale, Karlsen et al. [36] showed that strain heterogeneity, due to the low stacking fault energy of austenitic stainless steels, promotes strain localization during surface mechanical treatment, which in turn promotes crack initiation. Cracks propagate in depth, from 10 µm to 2 mm as a result of a tensile stress field acting on brittle highly deformed layers by machining in highly aggressive environment. However, compressive residual stresses in depth can slow down or stop the growth of these surface cracks. In any cases, the stress cracking corrosion provokes a

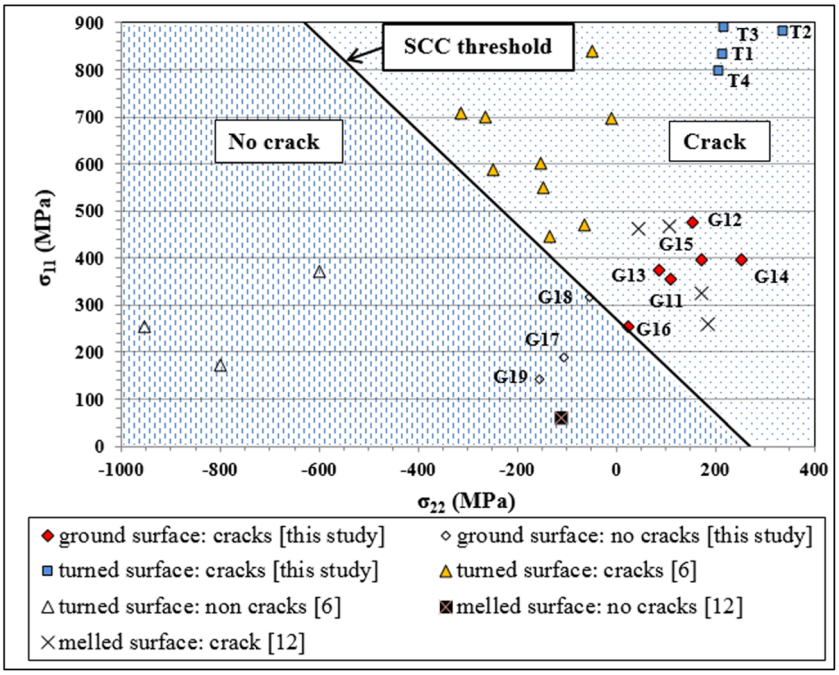

Fig. 11 Validation of SCC prediction criterion

significant redistribution of residual stresses characterized by an important relaxation phenomenon. This relaxation is mainly attributed to the effect of the chloride medium (up to 270%) than to the effect of the temperature (140 °C) which represents a relaxation rate lower than 20%, as indicated in column 6 of Table 6.

5 Conclusion

It has been demonstrated that machining processes, such as grinding and turning of AISI 316L austenitic stainless steel, induce near-surface modifications resulting in surface nanocrystallization, plastic deformation, and residual stress distribution. The revealed heterogeneity of machined surface properties is related to the scale of the stability of the cutting state. The surface residual stress is shown to be stable at the large millimeter scale for turned surface and at the very lower micrometric scale for the ground surface, due to the specific cutting conditions related to turning and grinding processes.

It has been established in this experimental study that the tensile residual stress distribution influences the SCC behavior of AISI 316L SS in $MgCl_2$ (40%) at 140 °C. The tensile residual stress directionality and level play a major role in the corrosion micro-crack initiation and in the resulting micro-crack network morphology. Therefore, a susceptibility to RSCC of AISI 316L SS in chloride medium is predicted using a criterion $\mathrm{tr}(\underline{\sigma}^{R}) < \left(\sigma^{\mathrm{RSCC}}_{\mathrm{threshold}}\right)_{\mathrm{MgCl_2;40\%}}$ with a threshold value of residual stress $\left(\sigma^{\mathrm{RSCC}}_{\mathrm{threshold}}\right)_{\mathrm{MgCl_2;40\%}} = 270$ MPa. This criterion has been validated for various stress distributions resulting from different machining conditions. Therefore, it should be used as a performing predictive tool of machining-induced susceptibility to RSCC.

References

1. Kumar PS, Acharyya SG, Rao SVR, Kapoor K (2017) Distinguishing effect of buffing vs. grinding, milling and turning operations on the chloride induced SCC susceptibility of 304L austenitic stainless steel. Mater Sci Eng A 687:193–199. https://doi.org/10.1016/j.msea.2017.01.079
2. Ben Fredj N, Sidhom H, Braham C (2006) Ground surface improvement of the austenitic stainless steel AISI 304 using cryogenic cooling. Surf Coat Technol 200(16):4846–4860. https://doi.org/10.1016/j.surfcoat.2005.04.050
3. Gürbüz H, Şeker U, Kafkas F (2017) Investigation of effects of cutting insert rake face forms on surface integrity. Int J Adv Manuf Technol 90(9):3507–3522. https://doi.org/10.1007/s00170-016-9652-7
4. Ma Y, Zhang J, Feng P, Yu D, Xu C (2018) Study on the evolution of residual stress in successive machining process. Int J Adv Manuf Technol 96(1):1025–1034. https://doi.org/10.1007/s00170-017-1542-0
5. Ben Rhouma A, Braham C, Fitzpatrick ME, Lédion J, Sidhom H (2001) Effects of surface preparation on pitting resistance, residual stress, and stress corrosion cracking in austenitic stainless steels. J Mater Eng Perform 10(5):507–514
6. Braham C, Ben Rhouma A, Lédion J, Sidhom H (2005) Effect of machining conditions on residual stress corrosion cracking of 316L SS. Mater Sci Forum 490-491:305–310. https://doi.org/10.4028/www.scientific.net/MSF.490-491.305
7. Nabil BF, Ben Nasr M, Ben Rhouma A, Sidhom H, Braham C (2004) Fatigue life improvements of the AISI 304 stainless steel ground surfaces by wire brushing. J Mater Eng Perform 13. https://doi.org/10.1361/15477020420819

8. Lyon KN, Marrow TJ, Lyon SB (2015) Influence of milling on the development of stress corrosion cracks in austenitic stainless steel. J Mater Process Technol 218:32–37. https://doi.org/10.1016/j.jmatprotec.2014.11.038
9. Ben Fredj N, Sidhom H (2006) Effects of the cryogenic cooling on the fatigue strength of the AISI 304 stainless steel ground components. Cryogenics 46(6):439–448. https://doi.org/10.1016/j.cryogenics.2006.01.015
10. Chang L, Burke MG, Scenini F (2018) Stress corrosion crack initiation in machined type 316L austenitic stainless steel in simulated pressurized water reactor primary water. Corros Sci 138:54–65. https://doi.org/10.1016/j.corsci.2018.04.003
11. Seifert HP, Ritter S (2016) The influence of ppb levels of chloride impurities on the strain-induced corrosion cracking and corrosion fatigue crack growth behavior of low-alloy steels under simulated boiling water reactor conditions. Corros Sci 108:148–159. https://doi.org/10.1016/j.corsci.2016.03.010
12. Zhang W, Fang K, Hu Y, Wang S, Wang X (2016) Effect of machining-induced surface residual stress on initiation of stress corrosion cracking in 316 austenitic stainless steel. Corros Sci 108:173–184. https://doi.org/10.1016/j.corsci.2016.03.008
13. Nishimura R, Maeda Y (2004) Metal dissolution and maximum stress during SCC process of ferritic (type 430) and austenitic (type 304 and type 316) stainless steels in acidic chloride solutions under constant applied stress. Corros Sci 46(3):755–768. https://doi.org/10.1016/j.corsci.2003.07.002
14. Nishimura R (2007) Characterization and perspective of stress corrosion cracking of austenitic stainless steels (type 304 and type 316) in acid solutions using constant load method. Corros Sci 49(1):81–91. https://doi.org/10.1016/j.corsci.2006.05.011
15. Beavers JA, Johnson JT, Sutherby RL (2000) Materials factors influencing the initiation of near-neutral pH SCC on underground pipelines. (40252):V002T006A041. https://doi.org/10.1115/ipc2000-221
16. Marteau J, Bouvier S (2016) Characterization of the microstructure evolution and subsurface hardness of graded stainless steel produced by different mechanical or thermochemical surface treatments. Surf Coat Technol 296:136–148. https://doi.org/10.1016/j.surfcoat.2016.04.010
17. Yan L, Yang W, Jin H, Wang Z (2012) Analytical modelling of microstructure changes in the machining of 304 stainless steel. Int J Adv Manuf Technol 58(1):45–55. https://doi.org/10.1007/s00170-011-3384-5
18. Cao Y, Ni S, Liao X, Song M, Zhu Y (2018) Structural evolutions of metallic materials processed by severe plastic deformation. Mater Sci Eng R Rep 133:1–59. https://doi.org/10.1016/j.mser.2018.06.001
19. Xu X, Zhang J, Liu H, He Y, Zhao W (2019) Grain refinement mechanism under high strain-rate deformation in machined surface during high speed machining Ti6Al4V. Mater Sci Eng A 752:167–179. https://doi.org/10.1016/j.msea.2019.03.011
20. Atmani Z, Haddag B, Nouari M, Zenasni M (2016) Combined microstructure-based flow stress and grain size evolution models for multi-physics modelling of metal machining. Int J Mech Sci 118:77–90. https://doi.org/10.1016/j.ijmecsci.2016.09.016
21. Turnbull A, Mingard K, Lord JD, Roebuck B, Tice DR, Mottershead KJ, Fairweather ND, Bradbury AK (2011) Sensitivity of stress corrosion cracking of stainless steel to surface machining and grinding procedure. Corros Sci 53(10):3398–3415. https://doi.org/10.1016/j.corsci.2011.06.020
22. Maranhão C, Paulo Davim J (2010) Finite element modelling of machining of AISI 316 steel: numerical simulation and experimental validation. Simul Model Pract Theory 18(2):139–156. https://doi.org/10.1016/j.simpat.2009.10.001
23. Martin M, Weber S, Izawa C, Wagner S, Pundt A, Theisen W (2011) Influence of machining-induced martensite on hydrogen-assisted fracture of AISI type 304 austenitic stainless steel. Int J Hydrog Energy 36(17):11195–11206. https://doi.org/10.1016/j.ijhydene.2011.05.133
24. Zhou N, Peng R, Pettersson R (2017) Surface characterization of austenitic stainless steel 304L after different grinding operations. Int J Mech Mater Eng 12. https://doi.org/10.1186/s40712-017-0074-6
25. Zhou N, Pettersson R, Lin Peng R, Schönning M (2016) Effect of surface grinding on chloride induced SCC of 304L. Mater Sci Eng A 658:50–59. https://doi.org/10.1016/j.msea.2016.01.078
26. Agrawal S, Joshi SS (2013) Analytical modelling of residual stresses in orthogonal machining of AISI4340 steel. J Manuf Process 15(1):167–179. https://doi.org/10.1016/j.jmapro.2012.11.004
27. Capello E (2005) Residual stresses in turning: Part I: Influence of process parameters. J Mater Process Technol 160(2):221–228. https://doi.org/10.1016/j.jmatprotec.2004.06.012
28. Zhou N, Peng RL, Pettersson R (2016) Surface integrity of 2304 duplex stainless steel after different grinding operations. J Mater Process Technol 229:294–304. https://doi.org/10.1016/j.jmatprotec.2015.09.031
29. Liu CR, Yang X (2001) The scatter of surface residual stresses produced by face-turning and grinding. Mach Sci Technol 5(1):1–21. https://doi.org/10.1081/mst-100103175
30. Chomienne V, Valiorgue F, Rech J, Verdu C (2016) Influence of part's stiffness on surface integrity induced by a Finish turning operation of a 15-5PH stainless steel. Procedia CIRP 45. https://doi.org/10.1016/j.procir.2016.02.331
31. Liu M, Takagi J-i, Tsukuda A (2004) Effect of tool nose radius and tool wear on residual stress distribution in hard turning of bearing steel. J Mater Process Technol 150(3):234–241. https://doi.org/10.1016/j.jmatprotec.2004.02.038
32. Martell J, Richard Liu C, Shi J (2014) Experimental investigation on variation of machined residual stresses by turning and grinding of hardened AISI 1053 steel. Int J Adv Manuf Technol 74. https://doi.org/10.1007/s00170-014-6089-8
33. Richard Liu C, Yang X (2007) The scatter of surface residual stresses produced by face-turning and grinding. Mach Sci Technol 5:1. https://doi.org/10.1081/mst-100103175
34. Smithey DW, Kapoor SG, DeVor RE (2000) A worn tool force model for three-dimensional cutting operations. Int J Mach Tools Manuf 40(13):1929–1950. https://doi.org/10.1016/S0890-6955(00)00017-1
35. Ding W, Zhang L, Li Z, Zhu Y, Su H, Xu J (2016) Review on grinding-induced residual stresses in metallic materials. Int J Adv Manuf Technol 88. https://doi.org/10.1007/s00170-016-8998-1
36. Karlsen W, Diego G, Devrient B (2010) Localized deformation as a key precursor to initiation of intergranular stress corrosion cracking of austenitic stainless steels employed in nuclear power plants. J Nucl Mater 406(1):138–151. https://doi.org/10.1016/j.jnucmat.2010.01.029